Localization of edge states at triangular defects in periodic MoS_2 monolayers

André Niebur,[1,*] Tommy Lorenz,[2] Michael Schreiber,[3] Gotthard Seifert,[1,†] Sibylle Gemming,[3] and Jan-Ole Joswig[1]
[1]*Theoretische Chemie, Technische Universität Dresden, 01162 Dresden, Germany*
[2]*Technische Thermodynamik, Technische Universität Dresden, 01162 Dresden, Germany*
[3]*Institute of Physics, TU Chemnitz, 09107 Chemnitz, Germany*

(Received 18 March 2021; accepted 18 May 2021; published 1 June 2021)

More than 150 different structural defects in periodic molybdenum disulfide (MoS_2) monolayers were investigated systematically for the present study by density-functional calculations. All defects were chosen to be triangular, but of different size and distance from one another. Molecular-dynamics simulations proved the defect stability against temperature effects. The energetic properties of the defective MoS_2 monolayers—-especially the density of states—-can be viewed as a combination of edge and bulk properties with the defect size being of dominating influence. A dependence on the defect-edge termination was present only in the very smallest defects. The definition of a localization parameter helps to characterize the grade of localization of the states. Finally, a strong influence of the defect distance on the electronic properties could not be observed, except for very small distances.

DOI: 10.1103/PhysRevMaterials.5.064001

I. INTRODUCTION

Molybdenum disulfide (MoS_2) has been known as a two-dimensional (2D) material for decades already. Nevertheless, it is still the subject of many current investigations, because of its interesting properties, possibility of easy production [1], and high potential for a broad range of applications. Being mechanically very robust [2,3], exfoliated MoS_2 monolayers are semiconducting in contrast to graphene, and the band gap is tunable by exposure to mechanical stress, e.g., to indentation [2,4]. Resulting applications are proposed in the areas of sensorics [5,6], nanoelectronics [2,7], catalysis [8,9], supercaps [9], piezoelectricity [10], and others. Especially, its flexibility and robustness predestine molybdenum disulfide for flexible electronics.

In addition to its particular nanomechanical properties, it turned out that edges of MoS_2 nanostructures show a unique catalytic activity, e.g., in desulfurization processes [8] or electrochemical hydrogen evolution [11]. These edges occur as boundaries in MoS_2 nanostrips or at defects in infinite monolayers. The latter can be produced through ion-beam techniques [12] or under electrochemical control [13]. MoS_2 monolayers produced in this way may contain numerous defects, which can strongly influence the properties.

The electronic properties of MoS_2 including electronic transport properties may be influenced severely by the introduction of edges into an intact structure, because these are very sensitive to defects. Especially, edges strongly influence the robustness of the conduction channels in a nontrivial way [14]. Moreover, edge defects in MoS_2 nanostructures even may cause magnetism. Li *et al.* [15] already investigated the magnetic properties of MoS_2 nanoribbons, and later on Yakobson and co-workers [16], for example, reported intrinsic magnetism of grain boundaries in 2D metal dichalcogenides. Controlled engineering processes, thus, may not only be restricted to the catalytic properties mentioned above, but might allow for tailoring electronic transport and magnetic properties as well.

The variety of structural defects in MoS_2 layers is particularly large. Influences on electronic and transport properties have been studied already (see, e.g., Ref. [17] and references therein). Therefore, the present work focuses on triangular defects in MoS_2 monolayers, which have been observed, when small holes form in electron-beam irradiated MoS_2 monolayers [18]. In that study, also the rim around large holes in MoS_2 exhibits straight segments, which follow the dense-packed crystal directions. Intermediate-sized pores and pores obtained by ion-beam irradiation are structurally less well defined, very reactive, and prone to the adsorption of other species [19–21]. Thus, MoS_2 assumes an intermediate position between hexagonal boron nitride with clearly defined triangular holes [19] and graphene with a large variety of different pores and also very different pore formation mechanisms [22,23].

The present paper aims at discussing new insights into properties of defected MoS_2 monolayers obtained by density-functional based methods. We have put the property dependence on defect sizes and defect distances into the focus of our study. In order to draw well-grounded and general conclusions, over 150 defect structures in periodic molybdenum disulfide (MoS_2) monolayers were constructed and investigated. Our construction procedure with respect to defect size and distance will be described in Sec. II.

*Present address: Leibniz Universität Hannover, Institut für Physikalische Chemie und Elektrochemie, Callinstr. 3A, 30167 Hannover, Germany.
†gotthard.seifert@tu-dresden.de

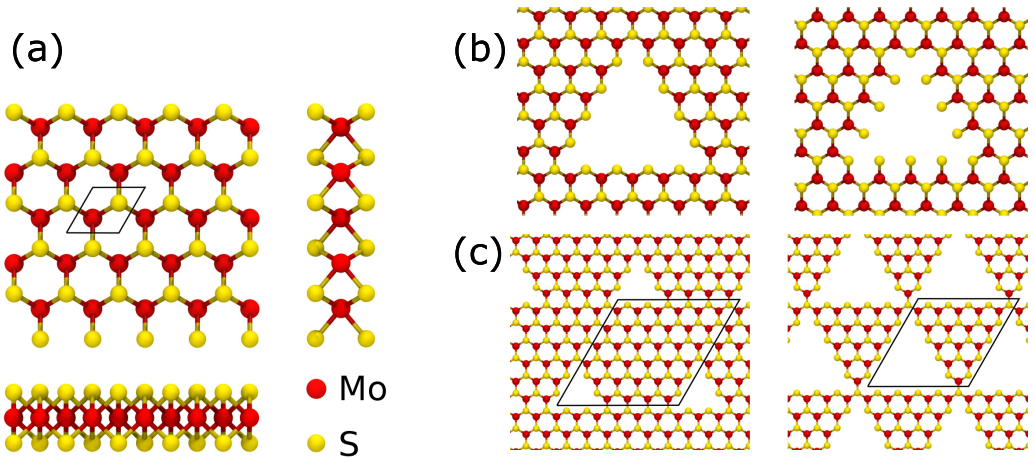

FIG. 1. (a) Two-dimensional MoS_2 monolayer in top and side views. (b) Two triangular defects ($m = 4$) with sulfur-poor (left) and sulfur-rich (right) saturations. (c) Two examples for periodic structures of a sulfur-poor (6,2) defect (left) and a sulfur-poor (5,4) defect (right) with highlighted periodic boundary conditions. Molybdenum and sulfur atoms are shown in red and yellow, respectively.

The analysis of the calculations was performed with a focus on different quantities: the structural changes with respect to defect-free MoS_2 were monitored; a localization factor was defined based on Mulliken charge analyses, which was used to characterize the grade of localization for electronic states of interest; the densities of states together with isosurface plots of the orbitals of interest were analyzed for all structures; and, finally, temperature stability of the defects was checked by the performance of molecular-dynamic simulations.

II. COMPUTATIONAL DETAILS

All calculations and simulations were carried out using the density-functional tight-binding (DFTB) method [24–26] as implemented in the program DFTB+. For geometry optimizations a tolerance of 10^{-5} hartree/Å was used, and molecular-dynamics simulations with a time step of 1 fs over a period of 10 ps were performed at 300 K using a Berendsen thermostat [27] with coupling constant of 0.1 ps.

The plain, optimized, and infinite MoS_2 monolayer was the origin for constructing the defective structures. Periodic boundary conditions were applied, whereby the layer was extended in the xy plane, and the z direction was set to 100 Å to avoid interactions between the periodic images. The defects were introduced by removing the respective atoms from the monolayer. Generally, triangular defects within an MoS_2 layer may be constructed in ways that lead to different edge saturations. These will be labeled as either sulfur rich or sulfur poor in the following (as explained in Fig. 1). The additional possibilities of creating unsaturated molybdenum edges or of studying mixed saturations were not considered here.

The defect size as well as the defect distance within the MoS_2 plane were systematically varied, the latter by choice of the periodic cell size. We introduce the following labeling: an (n, m) defect is located in a unit cell consisting of $n \times n$ repeated MoS_2 units and was constructed by removing a triangle with m molybdenum atoms at each edge.

We add that the optimized in-plane lattice parameters, which correspond to the nearest Mo-Mo distance, are 3.27 Å (converged with respect to number of k points and cell size). The resulting Mo–S bond length optimized within this cell is 2.45 Å, which agrees well with results of experiment [28] and other density-functional calculations [29,30].

The DFTB method was validated against density-functional calculations using the SIESTA code [31]. Exemplarily, we chose a defect-free (5,0) and a sulfur-poor defected (6,2) MoS_2 monolayer and compared the density of states around the Fermi level calculated for the optimized structure (with DFT and DFTB) and averaged over a 10-ps molecular-dynamics run (with DFTB). All results showed significant similarities especially with respect to the calculated band-gap size, and curve progressions (ratios of areas and heights of the density peaks), so that we are confident in applying the approximate, but fast and easy to handle DFTB method for this study.

III. RESULTS

The following discussion is based on the results of density-functional based calculations performed for a series of 150 defective monolayers. All structures were fully optimized. After optimization, the initial and optimized structures were compared in terms of atomic displacements and the total energy variations caused by the optimization procedure. Exemplarily, Fig. 2 shows the displacements as a function of the position in a sulfur-poor (15,5) MoS_2 monolayer. We can conclude that the initial structure is a good structural approximation. The displacements are generally very small, the largest being 0.16 Å and occurring in the vicinities of the defect corners and along the defect edges. As the defect introduces dangling bonds, larger displacements are expected at these places. On average, sulfur atoms show higher displacements than molybdenum atoms, because the z components of their positions change, especially in the vicinity of the defects. In contrast, the molybdenum atoms only change their in-plane position. A few atomic rows away from the edges, displacements drop to zero, indicating that the initial structure was a good approximation.

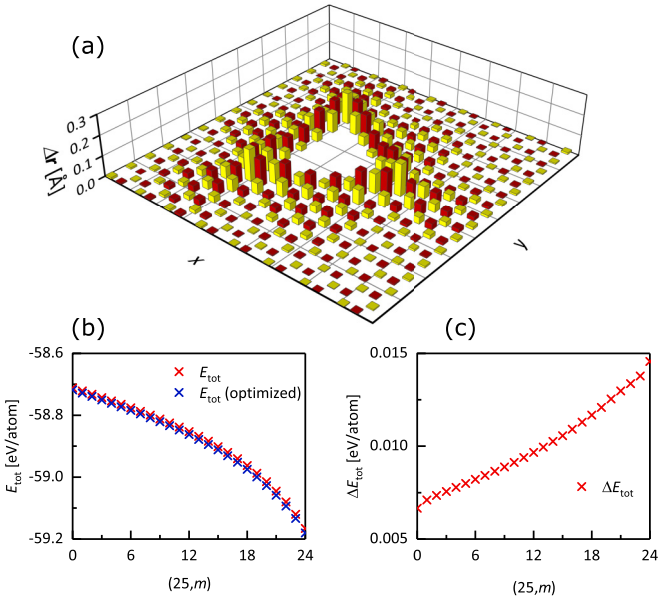

FIG. 2. (a) Absolute values of the atomic position changes during the geometry optimization of a sulfur-poor (15,5) MoS_2 monolayer as function of the position in the layer (xy plane, shown as a 45-Å-wide square cutout); color code as in Fig. 1. (b) Comparison of the total energies before and after optimization and (c) difference of the total energies before and after optimization, both as function of defect size m for constant cell size ($n = 25$).

Besides the structural changes, the total energy for a cell with 25 × 25 molybdenum atoms and increasing sulfur-poor defect size was monitored as well [Fig. 2(b)]. As both cell vectors have lengths of 81.8 Å the Γ-point approximation was used. The plot as a function of defect size shows only very small differences in total energies (per atom) for the initial and optimized structures. The difference plot [Fig. 2(c)] underlines this feature. Thus, both plots accentuate the fact that the initial MoS_2 structure is a good approximation to the defected structure and optimization leads to minor energy changes only. Note that the decrease of the total energy per atom with increasing defect size is originated in the stoichiometry, which is not constant. Nevertheless, the intact monolayer is expected to be the most stable system. The slight increase in the energy difference is a consequence of the increasing defect size, which goes alongside a larger amount of unsaturated atoms that show the highest displacements during optimization [see Fig. 2(a)].

In summary, it can be stated that an initially well-optimized structure is a good foundation for structures and energetics of defective monolayers. This is especially important for larger defects, where the number of atoms easily can exceed 10 000 atoms. Here, single-point calculations will be sufficient to uncover size-dependent trends in energy.

In the following we will draw our attention to the defect influence on the electronic structure with special focus on arising edge states. Usually, these states are localized at unsaturated edge or corner atoms in 2D materials or to surface atoms in 0D materials. The distinction between localized and delocalized states with help of visualized orbital isosurfaces is awkward, time-consuming, and imprecise. Therefore, we define a localization parameter Λ for quantification purposes. It is based on the Mulliken population analysis [32] and can be applied to both occupied and unoccupied molecular orbitals. The localization parameter Λ_j of molecular orbital j is

$$\Lambda_j = \sum_{i=1}^{N} p_{ij}^2,$$

where the sum includes the Mulliken gross-population contributions p_{ij} from all N atoms. Additionally, we define $P_j = \sum_{i=1}^{N} p_{ij}$, so that the localization parameter will be $\Lambda_j = P_j^2/N$ for a totally delocalized molecular orbital with equal atomic contributions p_{ij}, and $\Lambda_j = P_j^2$, if the molecular orbital is localized at a single atom of the system.

Derived from the previous consideration, the delocalization or participation number $N_{\mathrm{loc}} = P_j^2/\Lambda_j$ estimates the number of atoms, on which a particular molecular orbital j is localized, from the given localization parameter. Because this definition does not consider the system size, we normalize the resulting value with respect to the total number of atoms N in the system and obtain a so-called delocalization or participation ratio [33]

$$l_j = \frac{N_{\mathrm{loc}}}{N} = \frac{P_j^2}{N \sum_{i=1}^{N} p_{ij}^2}.$$

The relative specification allows comparison of different system sizes, e.g., $l_j = 0.01$ indicates the localization of the respective orbital to 1% of the atoms. However, we point out that the parameter is solely helping to interpret the Mulliken populations. Delocalization ratio and density of states of the defect-free monolayer are given in the Supplemental Material (Fig. S1) [34]. They show a high delocalization and regularity of the highest occupied and lowest unoccupied crystal orbitals, respectively HOCO and LUCO.

From the series of defective MoS_2 monolayers furnished with triangular defects of different sizes and interdefect distances, we exemplarily chose a sulfur-poor (20,4) MoS_2 structure. The defect has an edge length of 13 Å and the periodic images are approximately 52 Å apart from one another. The resulting delocalization ratios are displayed in Fig. 3(a) for occupied and unoccupied orbitals close to the Fermi level. As a result of the introduced defect, midgap states arise within the original HOCO-LUCO gap of the pristine layer. They occur between −3.5 and −2.0 eV of the absolute energy scale and are marked and numbered in the density of states in Fig. 3(b).

Comparative inspection of the density of states, the delocalization ratios, and the orbitals plots (Fig. S2 [34]) reveals that the orbitals closest to the Fermi level are the three degenerate and partially occupied orbitals nos. 1–3 and an unoccupied delocalized orbital no. 4. They are followed by four groups of three nearly degenerate orbitals each (nos. 5–7, 8–10, 11–13, 14–16) that are strongly localized to the defect edges. Their vertical node structure shows decreasing node numbers with increasing energy. These orbitals and their quantity are depending on the defect sizes. They can be identified clearly by delocalization ratios below 6%. As the resulting probabilities strongly decay between the periodic

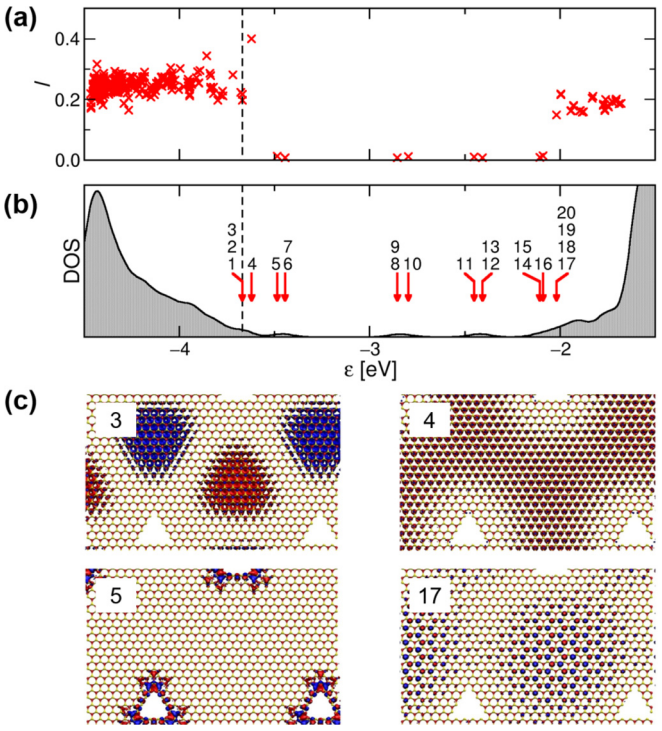

FIG. 3. Electronic properties of a sulfur-poor defective (20,4) MoS_2 monolayer. (a) Orbital delocalization ratios as function of orbital energy. (b) Density of states (black curve) with marked energy levels of the midgap states (arbitrary numbering). (c) Orbital isosurfaces for four crystal orbitals: HOCO (no. 3), LUCO (no. 4), a localized midgap state (no. 5), and a delocalized unoccupied orbital (no. 17). The Fermi level in (a) and (b) is indicated by a vertical dotted line. Visualizations of all midgap states are given in Fig. S2 [34].

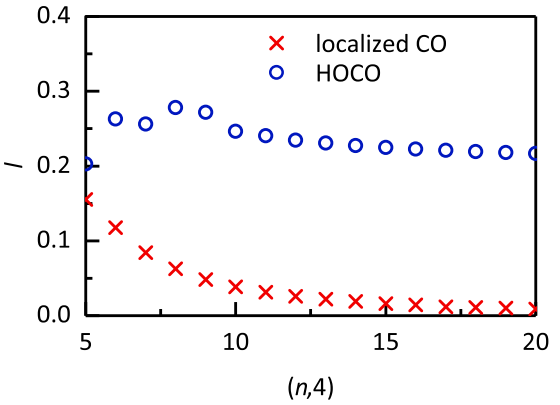

FIG. 4. Delocalization ratio as function of defect distance for the highest occupied crystal orbital (HOCO, blue) and the average of 12 localized frontier orbitals (localized CO, red) of a sulfur-poor (n,4) defect. The unit-cell size is given by integer multiples n of the unit-cell vector length.

images of the defects, charge transport cannot be expected to be conducted via these channels.

Categorization of orbitals by the introduced quantification tool is, thus, a helpful procedure, whose results here are verified by simultaneously inspecting the corresponding orbital plots. Delocalization ratios of $l < 6\%$ and $l > 15\%$ were found for strongly localized and mostly delocalized orbitals, respectively. On the other hand, orbitals with delocalization ratios in between are difficult to assign to either category.

Triangular defects may occur with different edge terminations: sulfur termination may be characterized as sulfur poor or sulfur rich [cf. Fig. 1(b)], whereas experimental evidence for molybdenum-terminated triangular hole structures is missing [18]. Therefore, we neither considered molybdenum termination nor mixed or irregular terminations here. The delocalization ratios of sulfur-poor and sulfur-rich structures (Fig. S3 [34]) show the same characteristics: in parts they lie entirely on top of each other; midgap states have the same low delocalization ratios, but differ in energy though. This is expected, because their energy is depending critically on the defect structure. Even orbitals in the hypothetical molybdenum-terminated structures yield comparable delocalization ratios, although a slightly different electronic structure.

The number of localized midgap states introduced by a triangular (n, m) defect is found to be proportional to the edge lengths. For each eliminated molybdenum atom at an edge, a set of unsaturated sulfur atoms remains introducing a midgap state. Thus, the number of states due to a triangular (n, m) defect is $3m$, e.g., 12 for the discussed (20,4) defect.

Whereas the number of edge states is independent of the defect distance, the delocalization ratio is not. Figure 4 shows the convergence of the delocalization ratios with increasing unit-cell size. In case of an $(m+1, m)$ defect, the structure is a corner-connected net of triangles, and the delocalization ratios of the HOCO and the localized states appear to be rather similar. This structure hosts the maximum number of regular defects, and all atoms are closely located to edges. The localized orbitals may appear delocalized at the same time due to the small unit cell. As a consequence, the defined delocalization ratio is less distinctive for high defect concentrations. For slightly larger cells, the distinction between localized and delocalized states is straightforward. Already a few rows of molybdenum atoms between the defects lead to visible convergence. In case of the (n,4) defect, $n = 10$ seems a reasonable choice, which leaves six molybdenum rows between the defects.

For examining the temperature dependence of the electronic structure, molecular-dynamics simulations were performed with the parameters summarized in Sec. II. The simulation temperature was set to 300 K. Structural snapshots from the resulting trajectories were taken, and single-point calculations of these structures were used to get a temperature-dependent density of states. In comparison to the density of states (DOS) of the respective optimized structure, these revealed that the midgap state energies were conserved, but that the DOS generally was smeared out over the gap energy range. This is a general and common observation.

As the Fermi energy of the studied structures roughly reflects the point at which the density of states starts to be dominated by localized states, it is plotted as a function of defect distance (Fig. 5). The defect distance was changed by using different unit-cell sizes for the same defect, and the data of 90 structures systematically were processed. With

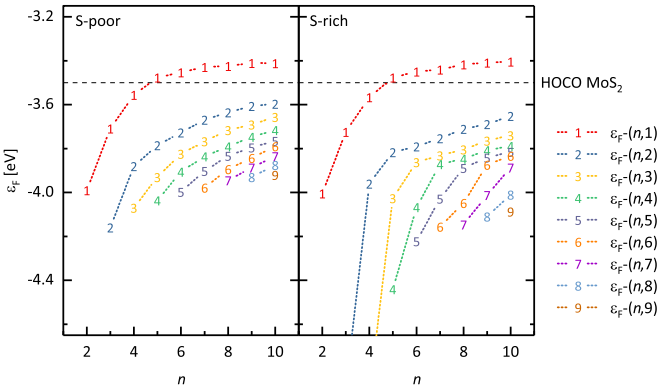

FIG. 5. Averaged Fermi energies resulting from molecular-dynamics simulations (sampled from MD simulation trajectories) for sulfur-poor (left) and sulfur-rich (right) triangular defects as function of unit-cell size n. The energy of the HOCO of the defect-free monolayer is indicated by horizontal dashed line in both diagrams.

increasing distance, the Fermi energy of defective monolayers converges to that of the intact monolayer. Thereby, the convergence depends on the defect size and distance, and for large defects the convergence is only an adumbrated trend due to the limitations of the set of structures.

At this point, we compare the edge states along the rim of the triangular defects and those along the circumference of triangular MoS_2 platelets because they have similar chemical environments, and earlier studies indicated that edge states in platelets play an important role in electronic excitations [4,35]. A defective MoS_2 monolayer with the highest possible defect concentration also can be viewed as a platelet net of an infinite number of triangular platelets connected via their edges. For such a kind of platelet net, a clear distinction between localized and delocalized states was not possible, because most atoms in a platelet are located close to an edge (see discussion of Fig. 4).

The densities of states of $(m + 1, m)$ defects are closely related to those of the corresponding platelets (see Fig. S5 [34]) underlining the platelet character of a platelet-net defect structure. Optical and catalytic properties of a highly defective monolayer should, therefore, be closely related to the respective platelet properties. For the density of states, this is found especially for large systems, because the influence of the corner atoms is negligible (see Fig. S4 [34]). Additionally, the influence of the termination on the energy levels vanishes in large systems and the Fermi energies asymptotically approach the same value (see Fig. S5 [34]).

IV. CONCLUSIONS

The electronic structure of a set of 150 periodic defective MoS_2 monolayers was calculated using a density-functional tight-binding approach, and the results were systematically analyzed. It turned out that good initial structure choices could be made by introducing the defects into a previously optimized MoS_2 monolayer. The structural and energetic changes upon optimization were generally small. Thus, the pristine MoS_2 monolayer structure is a well-suited approximation for the defective structure, and conclusions can be drawn already by single-point calculations on these initial structures.

The main focus was on the localization of midgap states, which are introduced through the defect. These states are clearly localized at the defect edges. The introduced participation ratio helps to quantify the grade of localization and makes it possible to distinguish between localized and delocalized states without consulting orbital plots.

The edge states of the triangular defects in the MoS_2 monolayer were then compared to those arising at edges of triangular nanoplatelets. For both structures, it could be shown that the energetic properties can be viewed as a sum of edge and bulk properties. This holds especially for the densities of states. It becomes apparent that the defect size is the dominating influence on the density of states. A dependence on the edge termination could be observed only for the smallest defects, so that it can be concluded that catalytic effects should be present in defects of either sulfur termination. The stability of the defects and their electronic structure with respect to temperature effects was shown with help of molecular-dynamics simulations.

Further attention is paid to the influence of the defect distance on their properties. We have quantitatively analyzed this dependence. It turns out that distant defects can be regarded as independent of each other. This is important knowledge for setting up electronic-structure calculations, e.g., for choosing the size of unit cells in periodic calculations and the interpretation of the arising results.

ACKNOWLEDGMENTS

The authors acknowledge computational time provided by Zentrum für Informationsdienste und Hochleistungsrechnen (ZIH) at TU Dresden for projects QDSIM and TransPheMat and fruitful discussions with Igor Baburin (Technische Universität Dresden) and Christian Wagner (Technische Universität Chemnitz).

[1] J. N. Coleman, M. Lotya, A. O'Neill, S. D. Bergin, P. J. King, U. Khan, K. Young, A. Gaucher, S. De, R. J. Smith *et al.*, Two-dimensional nanosheets produced by liquid exfoliation of layered materials, Science **331**, 568 (2011).

[2] T. Lorenz, M. Ghorbani-Asl, J.-O. Joswig, T. Heine, and G. Seifert, Is MoS_2 a robust material for 2D electronics? Nanotechnology **25**, 445201 (2014).

[3] T. Lorenz, J.-O. Joswig, and G. Seifert, Stretching and breaking of monolayer MoS_2 - an atomistic simulation, 2D Mater. **1**, 011007 (2014).

[4] J.-O. Joswig, T. Lorenz, T. B. Wendumu, S. Gemming, and G. Seifert, Optics, mechanics, and energetics of two-dimensional MoS_2 nanostructures from a theoretical perspective, Acc. Chem. Res. **48**, 48 (2015).

[5] C. Zhu, Z. Zeng, H. Li, F. Li, C. Fan, and H. Zhang, Single-layer MoS_2-based nanoprobes for homogeneous detection of biomolecules, J. Am. Chem. Soc. **135**, 5998 (2013).

[6] F. K. Perkins, A. L. Friedman, E. Cobas, P. M. Campbell, G. G. Jernigan, and B. T. Jonker, Chemical vapor sensing with monolayer MoS_2, Nano Lett. **13**, 668 (2013).

[7] H. Wang, L. Yu, Y.-H. Lee, Y. Shi, A. Hsu, M. L. Chin, L.-J. Li, M. Dubey, J. Kong, and T. Palacios, Integrated circuits based on bilayer MoS_2 transistors, Nano Lett. **12**, 4674 (2012).

[8] S. Gemming and G. Seifert, Nanocrystals: Catalysts on the edge, Nat. Nanotechnol. **2**, 21 (2007).

[9] Y. Yang, H. Fei, G. Ruan, C. Xiang, and J. M. Tour, Edge-oriented MoS_2 nanoporous films as flexible electrodes for hydrogen evolution reactions and supercapacitor devices, Adv. Mater. **26**, 8163 (2014).

[10] X. Song, F. Hui, T. Knobloch, B. Wang, Z. Fan, T. Grasser, X. Jing, Y. Shi, and M. Lanza, Piezoelectricity in two dimensions: Graphene vs. molybdenum disulfide, Appl. Phys. Lett. **111**, 083107 (2017).

[11] T. F. Jaramillo, K. P. Jorgensen, J. Bonde, J. H. Nielsen, S. Horch, and I. Chorkendorff, Identification of active edge sites for electrochemical H2 evolution from MoS_2 nanocatalysts, Science **317**, 100 (2007).

[12] M. Ghorbani-Asl, S. Kretschmer, D. E. Spearot, and A. V. Krasheninnikov, Two-dimensional MoS_2 under ion irradiation: From controlled defect production to electronic structure engineering, 2D Mater. **4**, 025078 (2017).

[13] J. Feng, K. Liu, M. Graf, M. Lihter, R. D. Bulushev, D. Dumcenco, D. T. L. Alexander, D. Krasnozhon, T. Vuletic, A. Kis, and A. Radenovic, Electrochemical reaction in single layer MoS_2: Nanopores opened atom by atom, Nano Lett. **15**, 3431 (2015).

[14] E. Erdogan, I. H. Popov, A. N. Enyashin, and G. Seifert, Transport properties of MoS_2 nanoribbons: Edge priority, Eur. Phys. J. B **85**, 33 (2012).

[15] Y. Li, Z. Zhou, S. Zhang, and Z. Chen, MoS_2 nanoribbons: High stability and unusual electronic and magnetic properties, J. Am. Chem. Soc. **130**, 16739 (2008).

[16] Z. Zhang, X. Zou, V. H. Crespi, and B. I. Yakobson, Intrinsic magnetism of grain boundaries in two-dimensional metal dichalcogenides, ACS Nano **7**, 10475 (2013).

[17] M. Ghorbani-Asl, A. N. Enyashin, A. Kuc, G. Seifert, and T. Heine, Defect-induced conductivity anisotropy in MoS_2 monolayers, Phys. Rev. B **88**, 245440 (2013).

[18] S. Wang, H. Li, H. Sawada, C. S. Allen, A. I. Kirkland, J. C. Grossman, and J. H. Warner, Atomic structure and formation mechanism of sub-nanometer pores in 2D monolayer MoS_2, Nanoscale **9**, 6417 (2017).

[19] H. J. Park, G. H. Ryu, and Z. Lee, Hole defects on two-dimensional materials formed by electron beam irradiation: Toward nanopore devices, Appl. Microsc. **45**, 107 (2015).

[20] R. Kozubek, M. Tripathi, M. Ghorbani-Asl, S. Kretschmer, L. Madauß, E. Pollmann, M. O'Brien, N. McEvoy, U. Ludacka, T. Susi, G. S. Duesberg, R. A. Wilhelm, A. V. Krasheninnikov, J. Kotakoski, and M. Schleberger, Perforating freestanding molybdenum disulfide monolayers with highly charged ions, J. Phys. Chem. Lett. **10**, 904 (2019).

[21] A. Niggas, J. Schwestka, S. Creutzburg, T. Gupta, D. Eder, B. C. Bayer, F. Aumayr, and R. A. Wilhelm, The role of contaminations in ion beam spectroscopy with freestanding 2D materials: A study on thermal treatment, J. Chem. Phys. **153**, 014702 (2020).

[22] R. A. Wilhelm and P. L. Grande, Unraveling energy loss processes of low energy heavy ions in 2D materials, Commun. Phys. **2**, 89 (2019).

[23] R. A. Wilhelm, E. Gruber, R. Ritter, R. Heller, S. Facsko, and F. Aumayr, Charge Exchange and Energy Loss of Slow Highly Charged Ions in 1 nm Thick Carbon Nanomembranes, Phys. Rev. Lett. **112**, 153201 (2014).

[24] D. Porezag, T. Frauenheim, T. Köhler, G. Seifert, and R. Kaschner, Construction of tight-binding-like potentials on the basis of density-functional theory: Application to carbon, Phys. Rev. B **51**, 12947 (1995).

[25] G. Seifert, D. Porezag, and T. Frauenheim, Calculations of molecules, clusters, and solids with a simplified LCAO-DFT-LDA scheme, Int. J. Quantum Chem. **58**, 185 (1996).

[26] G. Seifert and J.-O. Joswig, Density-functional tight binding—an approximate density-functional theory method, Wiley Interdiscip. Rev. Comput. Mol. Sci. **2**, 456 (2012).

[27] H. J. C. Berendsen, J. P. M. Postma, W. F. van Gunsteren, A. DiNola, and J. R. Haak, Molecular dynamics with coupling to an external bath, J. Chem. Phys. **81**, 3684 (1984).

[28] S. Helveg, J. V. Lauritsen, E. Lægsgaard, I. Stensgaard, J. K. Nørskov, B. S. Clausen, H. Topsøe, and F. Besenbacher, Atomic-Scale Structure of Single-Layer MoS_2 Nanoclusters, Phys. Rev. Lett. **84**, 951 (2000).

[29] F. A. Rasmussen and K. S. Thygesen, Computational 2D materials database: Electronic structure of transition-metal dichalcogenides and oxides, J. Phys. Chem. C **119**, 13169 (2015).

[30] T. Lorenz, D. Teich, J.-O. Joswig, and G. Seifert, Theoretical study of the mechanical behavior of individual TiS_2 and MoS_2 nanotubes, J. Phys. Chem. C **116**, 11714 (2012).

[31] J. M. Soler, E. Artacho, J. D. Gale, A. García, J. Junquera, P. Ordejón, and D. Sánchez-Portal, The SIESTA method for *ab initio* order-N materials simulation, J. Phys.: Condens. Matter **14**, 2745 (2002).

[32] R. S. Mulliken, Electronic population analysis on LCAO–MO molecular wave functions. I, J. Chem. Phys. **23**, 1833 (1955).

[33] F. Wegner, Inverse participation ratio in $2+\varepsilon$ dimensions, Z. Phys. B **36**, 209 (1980).

[34] See Supplemental Material at http://link.aps.org/supplemental/10.1103/PhysRevMaterials.5.064001 for further analysis of the defect-free MoS_2 monolayer and localized mid-gap states, information on the influence of different edge terminations, and a comparison between defective MoS_2 monolayers and MoS_2 platelets.

[35] T. Wendumu, G. Seifert, T. Lorenz, J.-O. Joswig, and A. N. Enyashin, Optical properties of triangular molybdenum disulfide nanoflakes, J. Phys. Chem. Lett. **5**, 3636 (2014).